

Hybrid Amplitude Ordinal Partition Networks for ECG Morphology Discrimination: An Application to PVC Recognition

Zhipeng Cai^{ID}, Member, IEEE, Caiyun Ma^{ID}, Graduate Student Member, IEEE,
Jianqing Li^{ID}, Senior Member, IEEE, and Chengyu Liu^{ID}, Senior Member, IEEE

Abstract—Various algorithms have emerged for automatic electrocardiogram (ECG) analysis, focusing on discerning subtle changes in arrhythmic morphology, especially premature ventricular contractions (PVCs). While ordinal partition networks (OPNs) have been effective in analyzing real-world time series data, conventional OPNs primarily concentrate on local ECG shapes, overlooking amplitude-level information. This study introduces an innovative method, absolute amplitude OPNs (AAOPNs), which incorporates amplitude-level variations (coarse-grained ECG) into ordinal patterns. These AAOPNs encompass all conceivable ordinal patterns as nodes, connected based on temporal sequences. Ten network measures are extracted from both OPNs and AAOPNs, capturing the shape and level-based PVCs characteristics. These measures are integrated into hybrid amplitude OPNs (HAOPNs) to construct support vector machine (SVM)-based PVCs recognition models. Evaluated on three baseline databases [Massachusetts Institute of Technology-Beth Israel Hospital arrhythmia database (96 587 beats), St. Petersburg Institute of Cardiological Techniques database (156 373 beats), and China Physiological Signal Challenge 2020 database (987 209 beats)], the proposed models demonstrate F1-scores of 97.02%, 93.06%, and 91.03% across databases in class-oriented evaluation, and 94.57%, 87.96%, and 88.89% in subject-oriented evaluation. Notably, the model achieves PVCs scores of 53 904 and 59 201 on the China Physiological Signal Challenge 2020 test set for the two evaluations, affirming its efficacy in PVCs recognition. This framework provides a versatile approach for detecting morphology anomalies in various physiological signals, such as heart sounds and pulses.

Index Terms—Complex networks (CNs), nonlinear dynamics time series analysis, ordinal partition networks (OPNs), premature ventricular contraction (PVC) detection, wearable electrocardiogram (ECG).

I. INTRODUCTION

ARRHYTHMIA identification and classification from electrocardiogram (ECG) plays a crucial role in the early

Manuscript received 10 November 2023; revised 4 March 2024; accepted 1 April 2024. Date of current version 13 June 2024. This work was supported in part by the National Natural Science Foundation of China under Grant 62001105 and Grant 62171123, in part by the China Postdoctoral Science Foundation under Grant 2023M730585, in part by the Jiangsu Funding Program for Excellent Postdoctoral Talent under Grant 2023ZB812, and in part by the Postgraduate Research and Practice Innovation Program of Jiangsu Province under Grant KYCX21_0089. The Associate Editor coordinating the review process was Dr. Lin Xu. (*Corresponding authors:* Zhipeng Cai; Chengyu Liu.)

The authors are with the State Key Laboratory of Bioelectronics, School of Instrument Science and Engineering, Southeast University, Nanjing 210096, China (e-mail: zhipeng@seu.edu.cn; chengyu@seu.edu.cn).

Digital Object Identifier 10.1109/TIM.2024.3400307

diagnosis of cardiovascular diseases. Clinically, the morbid state of the cardiovascular system can be estimated through subtle changes in ECG morphology and rhythm [1]. Therefore, many researchers and scientists use feature engineering and/or artificial intelligence to extract morphological and rhythmic information from ECG time series or beats to recognize cardiac arrhythmia. However, the nonlinear nature of the cardiovascular system prompts new approaches to explore its hidden nonstationary, chaotic, and complex dynamics information from ECGs for more accurate cardiac diagnosis.

Frequent premature ventricular contractions (PVCs) and multisource PVCs are prevalent arrhythmias linked to stroke and sudden cardiac death; early and accurate identification can provide crucial information for clinical treatment and intervention [2]. Recently, automatic PVC recognition techniques have evolved into two main categories: expert system (ES)-based and deep learning (DL)-based methods. ES methods utilize fixed thresholds on features derived from rhythmic intervals and morphological traits to categorize heartbeats. Li et al. [3] proposed a low-complexity data-adaptive approach achieving 93.4% sensitivity (*Se*) and 66.5% positive predictive value (PPV) for PVC recognition on MIT-BIH arrhythmia database (MIT-BIH-AR) database. Another approach, integrating heart rhythm and ECG shape changes through six QRS shape metrics, achieved 98.82% specificity (Sp) and 82.70% *Se* from the 2-lead MIT-BIH-AR Database [4]. Malek et al. [5] improved template-matching for PVC recognition, attaining 92.01% *Se*, 99.24% Sp, and 98.84% accuracy (Acc) on part of MIT-BIH-AR.

DL-based methods automatically extract high-dimensional features, suited for big data scenarios. Yıldırım et al. [6] introduced a 1D-convolutional neural network (CNN) model, reaching 91.33% Acc across 17 classes in MIT-BIH-AR. Pławiak [7] enhanced metrics to 91.40% *Se* and 98.99% Acc using genetic ensembles of SVM-based classifiers. An improved gated recurrent unit embedded within a CNN framework achieved 98.00% *Se*, 97.80% Sp, and 97.90% Acc on MIT-BIH-AR [8]. Despite the efficacy of ES and DL methods on diverse datasets, ES-based features are concrete and noise-prone, while DL-based features are indigestible. Given cardiac complexity, extracting features aligning underlying physiological mechanisms with concrete attributes holds significance.

As a nonlinear dynamics time series analysis method, complex networks (CNs) have been employed in a variety of

physical and engineering systems, and a variety of network measures are used to characterize their underlying dynamics. Over the past decade, several graph-based time series characterization approaches have been proposed to reveal nontrivial information about the series itself. A visibility graph maps time series into CN based on the visibility criterion between two corresponding data, and it is effective in bearing fault diagnosis [9] and brain injury localization and size estimation [10]. Recurrence networks, converting time series into phase space to unveil geometric characteristics of the underlying system and its extensions of cross-recurrence networks and joint recurrence networks have been applied in thermoacoustic instability [11] and brain dynamics [12]. Transition networks connect embedded points in phase space based on their temporal succession on the trajectory, and have been employed in the fatiguing contractions analysis of muscles [13] and sudden changes quantification in dynamical systems [14]. Visibility graph and recurrence network approaches can distinguish between periodic and chaotic dynamics under noise-free conditions, but they always confront measurement errors in real-world data (especially for small thresholds (ϵ) in recurrence networks) [15]. Transition networks are well suited for exploring the causal evolution of the studied system (that is, regions in phase space), but they may lose morphological information about tiny amplitude changes [16].

Recently, a novel variant of transition networks, known as ordinal partition networks (OPN), has emerged, directly converting time series into CN using the parameter-free Bandt–Pompe symbolization method [17]. OPN and its adaptations have found application in real-world time series analysis. For instance, RR intervals from premature and full-term newborns were OPN-mapped, utilizing permutation, conditional, and global node entropies to discern autonomic nervous system maturation in newborns [18]. Additionally, Pessa et al. [19] extended the ordinal network algorithm to images, employed in liquid crystals to distinguish doping concentrations and predict sample temperatures during chiral mesophase induction. Weighted-directed OPNs were constructed for multivariate time series using first-order differences, employing entropy-based metrics to characterize ordinal partition transition dynamics and phase synchronization paths [20]. The OPN method provides CN construction devoid of explicit embedding procedures, outperforming amplitude-binning methods in capturing subtle amplitude variations.

While traditional OPNs are able to capture local waveform shapes, such as the rise/fall of the waveform, they ignore amplitude details based on global shapes, such as the deformed QRS complex in PVC. Addressing this limitation, Sun et al. [21] devised a solution by integrating the amplitude levels of sliding windows at distinct time points with their corresponding ordinal patterns, effectively characterizing windowed segments. Inspired by Sun’s work, we introduce absolute amplitude OPN (AAOPN) to extract amplitude level-based information related to global ECG waveform and combine it with the shape-based information extracted by OPN to construct hybrid amplitude OPN (HAOPN), thereby enhancing the accuracy of ECG morphology discrimination. In detail, we initially transform original PVC heartbeats

into a set of ten fixed symbols (0–9), representing distinct morphological features through a static coarse-grained symbolic representation. This initial encoding effectively captures the intricate PVC morphology within the topology of CNs. Building upon this, we further refine OPNs to map absolute amplitude symbols of windowed segments, creating an AAOPN. Subsequently, we integrate information from both the OPN and AAOPN, yielding a HAOPN. This comprehensive HAOPN provides a nuanced and detailed insight into the morphological characteristics of ECG signals. The next phase involves training support vector machine (SVM)-based PVC recognition models using the derived HAOPN measures.

Our method is meticulously trained on the MIT-BIH arrhythmia (MIT-BIH-AR) dataset and rigorously tested on datasets from the St. Petersburg Institute of Cardiological Technics (INCART) and the China Physiological Signal Challenge 2020 (CPSC2020). The primary objective is to bridge the existing gap between the tangible yet noise-prone features of ES-based methods and the less interpretable features of DL-based methods. By leveraging hybrid amplitude information, our approach strives to offer a solution that is not only more interpretable but also resilient to noise, thereby contributing to a more accurate and reliable PVC recognition system for ECG signals.

The primary contributions of this study can be outlined as follows:

- 1) Introduction of the innovative concept of AAOPN, which encodes absolute amplitude-related information within CNs; the measures aid in detecting morphological abnormalities in the recognition of PVC.
- 2) Pioneering utilization of CN (particularly OPNs) for heartbeat identification signifies a notable stride in single-heartbeat categorization, demonstrating remarkable progress from the standpoint of network dynamics.
- 3) Thorough reannotation of the training dataset on a beat-by-beat basis, offering comprehensive annotations (precise R-peak locations and types) for the CPSC2020 training dataset.

II. METHODS

A. Materials

1) *MIT-BIH-AR Database*: The training set comprises lead II ECG signals from the MIT-BIH-AR database. It encompasses 48 two-channel ambulatory 30-min ECG recordings, obtained from 47 subjects ($F_s = 360$ Hz). Notably, records with paced beats (102, 104, 107, and 217) were excluded following the Association for the Advancement of Medical Instrumentation recommendations. Focusing on ECG morphological abnormalities, only PVC and normal (N) beats are considered. Patient-specific PVC recognition model evaluation involves dividing the MIT-BIH-AR database into the training set DS1 (including 101, 106, 108, 109, 112, 114, 115, 116, 118, 119, 122, 124, 201, 203, 205, 207, 208, 209, 215, 220, 223, 230) and testing set DS2 (including 100, 103, 105, 111, 113, 117, 121, 123, 200, 202, 210, 212, 213, 214, 219, 221, 222, 228, 231, 232, 233, 234) (as shown in Table I).

2) *INCART Database*: The INCART database comprises 75 12-lead annotated ECG recordings. These recordings are

TABLE I
DETAILED INFORMATION OF THE DATABASES USED IN THIS STUDY

	Database	ECG length	# PVC beats	# Total beats	Fs (Hz)	# Record	Remarks
Train	MIT-BIH-AR	30 min	6,983	96,587	360	44	--
	DS1		3,774	49,414		22	--
	DS2	30 min	3,209	47,173	360	22	--
Test	INCART	30 min	18,362	156,373	257	75	--
	CPSC2020-Train	~24 h	42,075	895,711	400	10	Posted on the official website [22] Labeled by this work [23]
			43,174	987,209			

sampled at 257 Hz and last for 30 min each. The beat annotations within this database have undergone rigorous correction, informed by the results of an automated algorithm. In our study, we direct our attention to PVC and N beats extracted from lead II ECG recordings (as indicated in Table I).

3) *CPSC2020 Database*: CPSC2020 focuses on PVC and supraventricular premature beat identification from 24-h single-lead ECG recordings. Training data (CPSC2020-Train) includes ten single-lead wearable ECG recordings with pathological arrhythmias and signal issues. PVC and supraventricular beat locations are accessible on the official website. With committee guidance, we meticulously reannotated the training set beat by beat. Detailed annotation of QRS complexes on high-quality segments is available. Details of CPSC2020-Train (pre- and post-reannotation) are in Table I. The test set (CPSC2020-Test) comprises similar ECG recordings, but it's not publicly available.

B. Ordinal Networks From Time Series

To reduce noise in ECG signals, particularly in dynamic ECGs, a second-order forward and backward Butterworth bandpass filter (0.1–45 Hz) is utilized for baseline drift and high-frequency noise removal [24]. Filtered signals are then normalized to $[-1, 1]$ before QRS locations, using a unique quasi-periodic cardiovascular signals detector [25]. Heartbeats are segmented around R peaks as per experimental needs, followed by extraction of OPN and AAOPN features for PVC recognition via SVM models. Notably, each record in CPSC2020 is partitioned into 30-min segments before preprocessing.

1) *Ordinal Partition Network*: To generate an OPN for a uniformly sampled time series $x = \{x_1, x_2, x_3, \dots, x_N\}$, where N is the time series length, the data are initially partitioned into m -dimensional ordinal patterns with a time lag τ . Each embedded vector $v_i = \{x_i, x_{i+\tau}, x_{i+2\tau}, \dots, x_{i+(m-1)\tau}\}$ is mapped to an ordinal pattern $s_i = (\pi_1, \pi_2, \pi_3, \dots, \pi_m)$ based on the element amplitude ordering: $x_{(i-1)+\pi_1} \leq x_{(i-1)+\pi_2} \leq \dots \leq x_{(i-1)+\pi_m}$, where $\pi_k \in \{1, 2, \dots, m\}$ and $\pi_k \neq \pi_l \iff k \neq l$ such that $\pi_k < \pi_l \iff x_k > x_l$, for all $x_k, x_l \in v_i$. To obtain a set of unique ordinal patterns $S = \{s_1, s_2, \dots, s_{N-(m-1)\tau}\}$, if two elements of v_i are equal in value, the rank for these elements is assigned based on their appearance order in the vector, that is $\pi_k < \pi_l \iff k < l$ for $x_k = x_l$. Obviously, for a given embedding dimension m , the total number of all possible ordinal patterns is $m!$ Subsequently, links between two ordinal patterns (nodes) are allocated based on their temporal succession. To construct an OPN, each element of all possible ordinal patterns $\{s_i\}_{i=1}^{m!}$ represents a node in the network $G = \{V, E\}$,

and E is the set of edges drawn according to the succession between node pairs. The mathematical representation of G is an adjacency matrix A ($m! \times m!$), whose element $a_{i,j}$ stands for the link between node i to node j .

For a more intuitive illustration of the OPN construction procedure, we assume a simple normalized time series $x = \{-0.89, 0.39, 0.29, 0.91, 0.11, 0.25, 0.31, -0.09, 0.18, -0.16\}$ with embedding dimension $m = 3$ and time lag $\tau = 2$ (OPN construction procedure in the left part of Fig. 1). The embedded vectors are $v = \{(-0.89, 0.29, 0.11), (0.39, 0.91, 0.25), (0.29, 0.11, 0.31), (0.91, 0.25, -0.09), (0.11, 0.31, 0.18), (0.25, -0.09, -0.16)\}$, and their corresponding ordinal patterns are $S = \{(1, 3, 2), (3, 1, 2), (2, 3, 1), (3, 2, 1), (1, 3, 2), (3, 2, 1)\}$. For instance, the first partition of the time series is $v_1 = (-0.89, 0.29, 0.11)$ which fulfills the order $x_{(i-1)+1} \leq x_{(i-1)+3} \leq x_{(i-1)+2}$ ($i = 1$), and thereby its ordinal pattern is $s_1 = (1, 3, 2)$. Then, repeat these steps until all the vectors are considered, and the ordinal patterns S are obtained. As the embedding dimension m is 3, all the nodes in the OPN are $V = \{(1, 2, 3), (1, 3, 2), (2, 1, 3), (2, 3, 1), (3, 1, 2), (3, 2, 1)\}$. From S , the first succession is $\{V_2, V_5\}$, so there is a link between the corresponding nodes V_2 and V_5 , namely, the adjacency matrix element $a_{2,5} = 1$. Note that only four nodes $\{V_2, V_4, V_5, V_6\}$ occur in this example and the remaining two nodes $\{V_1, V_3\}$ are absent. Therefore, the element $a_{i,j}$ associated with nodes $\{V_1, V_3\}$ are filled by 0, which are not illustrated in Fig. 1 for simplicity.

2) *Absolute Amplitude OPN*: The initial step of AAOPN involves symbolizing the time series, capturing coarse dynamic trends while sacrificing detailed morphological variations. We adopt the equal interval univariate symbolic approach to convert an N length time series ($x = \{x_i, i = 1, 2, \dots, N\}$) into a sequence of symbols. The entire range of x is divided into α regions, each associated with a specific symbolic value.

Data points ($x(i)$) are replaced with symbols based on the region they belong to. Specifically, a ten-symbol (0–9) global symbolization is applied to the normalized time series, as in the following equation:

$$y_i = \begin{cases} 9, & 0.8 \leq x_i \leq 1 \\ 8, & 0.6 \leq x_i < 0.8 \\ \vdots & \vdots \\ 0, & -1 \leq x_i < -0.8. \end{cases} \quad (1)$$

Subsequently, the obtained symbolic series $y = \{y_i, i = 1, 2, \dots, N\}$ is embedded in a similar manner as the traditional

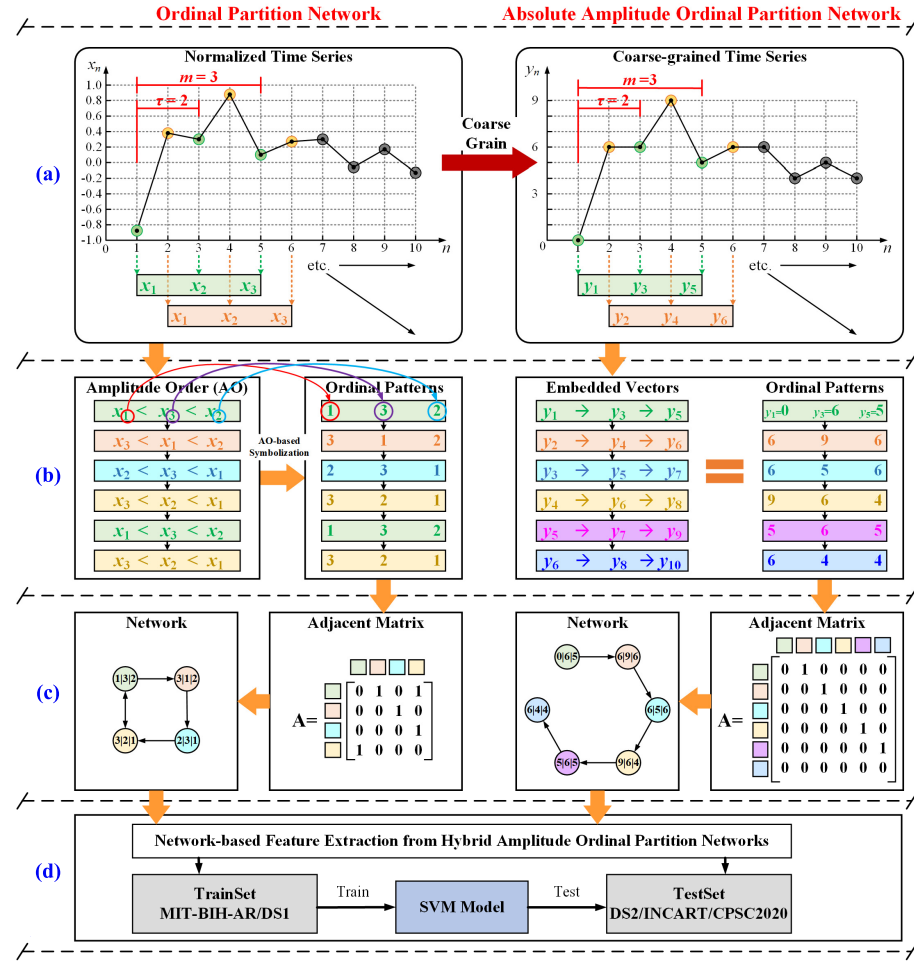


Fig. 1. Protocol of this study. (a) Time series and windowed segmentation, (b) ordinal symbolization, (c) network construction, and (d) SVM-based learning.

OPN. However, in AAOPN, the embedded vectors $v_i = \{y_i, y_{i+\tau}, y_{i+2\tau}, \dots, y_{i+(m-1)\tau}\}$ are used as ordinal patterns $s_i = (\pi_1, \pi_2, \pi_3, \dots, \pi_m)$, where $y_k = \pi_k$ and $k = i + (m-1)\tau$. With a given α and m , the total number of possible absolute amplitude ordinal patterns in AAOPN is α^m . Like OPN, all these ordinal patterns represent nodes within AAOPN, and their connections are determined by the temporal succession between pairs of nodes.

Review the example in OPN, the coarse-grained ten-symbol series of x is $y = \{0, 6, 6, 9, 5, 6, 6, 4, 5, 4\}$, and its corresponding ordinal patterns ($m = 3$ and $\tau = 2$) are $S = \{(0, 6, 5), (6, 9, 6), (6, 5, 6), (9, 6, 4), (5, 6, 5), (6, 4, 4)\}$. The construction procedure of AAOPN is depicted in the right portion of Fig. 1. With an embedding dimension $m = 3$, the AAOPN's node count for the ten-symbol series becomes $10^3 = 1,000$. The first succession in S means that there is a link between node (0,6,5) and node (6,9,6). Similarly, the element $a_{i,j}$ associated with absent nodes are set to 0.

C. Hybrid Amplitude-Based Learning Framework

1) **Network-Based Measures:** Ten network measures are extracted in this study.

a) **Average degree:** The degree of a node is defined as the number of edges connected to it, and the average degree in the

following equation is the mean value of all nodes' degree [24]:

$$\text{Average Degree} = \frac{1}{N} \sum_{n=1}^N d_n \quad (2)$$

where N is the total number of nodes and d_n is the degree of node n .

b) **Average clustering coefficient:** The cluster coefficient of a node is the ratio of all triangles involving that node to the number of connected triples centered on it, and the average clustering coefficient in the following equation of a network is the mean value of all nodes' clustering coefficients [26]:

$$\text{Average Clustering Coefficient} = \frac{1}{N} * \sum_{i \in V} \frac{e_i}{k_i * (k_i - 1)} \quad (3)$$

where e_i is the actual number of edges between all the couples of neighbors of node i , and $k_i * (k_i - 1)$ is the maximum possible number of edges between all the k_i neighbors of node i , V is the set of N nodes.

c) **Graph energy:** Graph energy in the following equation is defined as the sum of the absolute values of the real components of the eigenvalues (λ_i) of the graph [27]:

$$\text{Graph Energy} = \sum_i |\lambda_i|. \quad (4)$$

d) Transitivity: The transitivity in the following equation is the ratio between the triangle numbers and the connected triple numbers in a graph [26]. This calculation aims to derive the global information of the cluster coefficient in the network:

$$\text{Transitivity} = \frac{3 * \text{number of triangles in graph}}{\text{number of connected triples in graph}}. \quad (5)$$

e) Link density: Link density in the following equation is the ratio between the edges number and the maximum possible number of edges ($N * (N - 1)/2$) [28]:

$$\text{Link Density} = \frac{\sum_{i=1}^N \sum_{j=1}^N e_{ij}}{N * (N - 1)/2}. \quad (6)$$

f) Average degree centrality: Average degree centrality is calculated as the ratio of the number of nodes connected to the current node to the total number of nodes in the network [29]

$$\text{Average Degree Centrality} = \frac{1}{N} \sum_{i=1}^N \frac{\sum_{j=1}^N e_{ij}}{N - 1}. \quad (7)$$

g) sMetric: The sMetric in the following equation is the sum of products of nodal degrees across all edges [30]:

$$\text{sMetric} = \sum_{i,j=1}^N d_i * d_j. \quad (8)$$

h) Permutation entropy: Permutation entropy [31] is the Shannon entropy of the ordinal patterns S

$$\text{Permutation Entropy} = - \sum_i p_i \log p_i \quad (9)$$

where the probabilistic mass function $P(s = s_i) = p_i$ for $s_i \in S$ is estimated by counting the relative occurrence of each symbol in the symbolic dynamics S .

i) Conditional permutation entropy: Conditional permutation entropy [31] is defined as the anticipated value of the average entropy of node i , considering the stationary distribution of the ordered network. Here, we refer to the concept of node entropy defined in [32], which is the internal summation as follows:

$$\text{Conditional Permutation Entropy} = \sum_i \left(-p_i \sum_j p_{i,j} \log p_{i,j} \right) \quad (10)$$

where $p_{i,j}$ is the probability of a transition from s_i to s_j as estimated from S .

j) Global node entropy: The global node entropy [31] is the transitional complexity of S represented as the average over the network and determined by the stationary distribution estimated by (12)

$$\text{Global Node Entropy} = - \sum_i p_i \sum_j p_{i,j}^T \log p_{i,j}^T \quad (11)$$

where $p_{i,j}^T$ is the element of the modified stochastic matrix P^T of an ordinal network that excludes the possibility of self-loops. Therefore, it has elements $p_{i,j}^T$

$$p_{i,j}^T = \begin{cases} 0, & \text{if } i = j \\ \frac{a_{i,j}}{\sum_{j,j \neq i} a_{i,j}}, & \text{if } i \neq j. \end{cases} \quad (12)$$

2) Hybrid Amplitude Feature Extraction and Model Construction: The hybrid amplitude features, including the segment shape information from OPN and the amplitude level information from AAOPN, are used as the input of an SVM classifier. The SMOTE is used as the data balance method. A radial basis function is selected with two parameters: the error penalty factor C and the kernel width Gamma. The grid search approach is employed to optimize the parameters with C range as [0.1, 1, 10, 100, 1000] and the Gamma range as [0.0001, 0.001, 0.01, 0.1, 1]. Then, all grid points of (C , Gamma) are tested and the one that realizes the highest fivefold cross-validation accuracy is chosen as the best parameter to train the model. Note that the hybrid amplitude features are abbreviated as HAOPN for convenience.

From the definition of OPN and AAOPN, the embedding dimension m controls how finely the time series is partitioned. Larger m may afford a more accurate network model encoding the nonlinear dynamics of time series, while may also boost the computational complexity of network-based measures [33]. From above, the node numbers of OPN and AAOPN are $m!$ and 10^m , respectively. To ensure the comparability of OPN and AAOPN network size, their embedding dimensions are set to 5 and 2, resulting $5! = 120$ and $10^2 = 100$ nodes. It is worth noting that all the experiments in this study are based on these parameter settings.

3) Performance Evaluation: In this article, we employ three widely recognized metrics to assess the proposed algorithm's performance: F1-score (F_1), Se, and PPV. Four indexes [true positive (TP), true negative (TN), false positive (FP), and false negative (FN)] are generated, and F_1 , Se, PPV are defined as $F_1 = 2 * \text{TP} / (2 * \text{TP} + \text{FP} + \text{FN})$, $\text{Se} = \text{TP} / (\text{TP} + \text{FN})$, and $\text{PPV} = \text{TP} / (\text{TP} + \text{FP})$, respectively. All experiments are conducted on AMD EPYC 7542 32-core CPU with 64 GB RAM. Our QRS detector exhibited strong performance across the MIT-BIH-AR, INCART, and CPSC2020-Train databases, achieving Se values of 99.38%, 99.45%, 97.76%, PPV values of 99.56%, 99.32%, 99.05%, and F_1 values of 99.47%, 99.39%, and 98.40%.

For PVC recognition, we explore both "class-oriented" and "subject-oriented" evaluation methods. In the "class-oriented" approach, the MIT-BIH-AR database is split into 7:3 training and testing sets. We train PVC recognition models on the training data using fivefold cross-validation and assess performance on the testing data. Notably, the folds during cross-validation are patient-stratified. To ensure realism, we also conduct a "subject-oriented" evaluation. The MIT-BIH-AR database is divided into DS1 (training) and DS2 (testing). DS1 is for model training and optimization, while DS2 is for testing. To assess generalization, OPN-SVM, AAOPN-SVM, and HAOPN-SVM models are evaluated on INCART and CPSC2020 databases.

III. EXPERIMENTS AND RESULTS

A. Ordinal Networks From ECG Segments

To provide a clear illustration of the distinction between OPN and AAOPN, Fig. 2 depicts the constructed networks for typical N beats and two distinct types of PVCs from

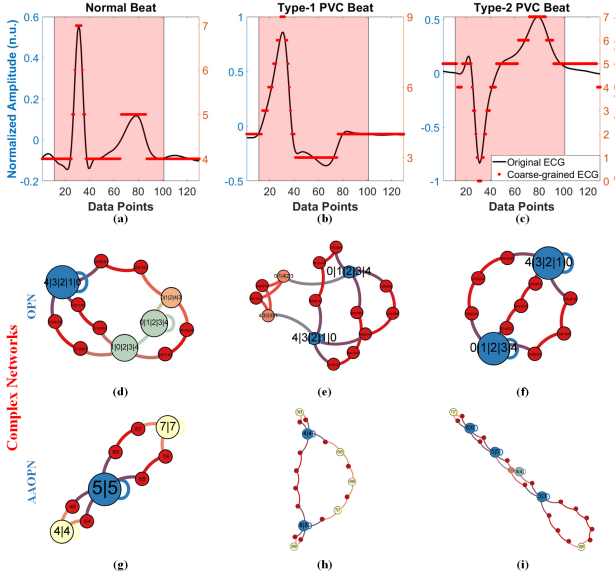


Fig. 2. Comparison between OPN and AAOPN on typical N beats and PVC beats. (a)–(c) show typical ECG signals and corresponding symbolic series, (d)–(f) illustrate constructed OPN, and (g)–(i) depict constructed AAOPN. The networks are drawn by the free software Gephi with a “ForceAtlas 2” layout, the size and color of a node correspond to its degree.

lead II ECG signals, utilizing a time lag of $\tau = 1$. The normalized ECGs, shown in Fig. 2(a)–(c), reveal distinct patterns. In contrast to N beats, type-1 PVCs exhibit taller and broader malformed QRS complexes, while type-2 PVCs display smaller QRS waveforms accompanied by prominent negative waves. Consequently, the coarse-grained time series of N beats manifest fewer stable symbolic states during QRS complexes than PVC beats. This phenomenon arises from PVCs’ wider QRS complexes, resulting in reduced transition rates between symbolic states and extended durations for each state. Moreover, the elevated QRS complexes in type-1 PVCs and the substantial negative waves following QRS complexes in type-2 PVCs enhance their intersections during global symbolization, heightening the diversity of symbolic states.

The construction of OPNs with only effective nodes is described for the episodes highlighted in red in Fig. 2(d)–(f). Notably, the node size and color correspond to their respective node degrees, with the number of effective nodes within the type-1 PVC OPN exceeding those of the other two typical cases. In particular, the nodes labeled “0|1|2|3|4” and “4|3|2|1|0” exhibit higher degrees than the remaining nodes in the OPNs of all three typical beats. This observation indicates the increased importance of nodes representing positive and negative linear ordinal patterns in capturing essential features of the data. Additionally, this suggests a potential challenge, as OPNs may use the same ordinal patterns for different waveforms, potentially masking amplitude-level information in distinct cases.

The AAOPNs depicted in Fig. 2(g)–(i) for the three representative beats reveal a higher number of effective nodes in PVCs compared to N beats. Nodes formed by identical symbols exhibit higher degrees and often play crucial roles

as key nodes within the network. These key nodes align with characteristic sub-waves in the original ECG waveform, such as the baseline, T wave, and QRS complexes peak (visible in N and type-1 PVC) or the deep negative wave valley (seen in type-2 PVC). Nodes situated between these key nodes indicate transitions between sub-waves, present as symbol pairs with ascending and descending orders. This underscores AAOPN’s ability to encode amplitude-related details within a CN, offering insights consistent with clinical diagnosis interpretations.

B. HAOPN-Based PVC Recognition

Ten network-based measures were extracted from OPN ($\tau = 1$, $F_s = 200$ Hz, $N = 0.1$ s * F_s) and AAOPN ($\tau = 1$, $F_s = 200$ Hz, $N = 0.1$ s * F_s) on MIT-BIH-AR database. These, along with their combination (HAOPN), were employed for training PVC recognition models (OPN-SVM, AAOPN-SVM, and HAOPN-SVM) via SVM. To assess the efficacy of OPN- and AAOPN-based measures in PVC recognition, these measures were z -score normalized, and their distributions between N and PVC cases were depicted in Fig. 3(a) and (b). AAOPN-based measures displayed more pronounced discrepancies between N and PVC than OPN-based measures. To quantify these differences, the Wilcoxon rank sum test was applied to each measure. Significance ($p < 0.05$) was marked with red “*”, and high significance ($p < 0.01$) was marked with red “**”.

Notably, nearly all p -values derived from AAOPN-based measures were <0.05 (excluding graph energy), while fewer OPN-based measures showed significant differences. Fig. 3(c) and (d) showcases the distribution of randomly selected typical measures (transitivity and average clustering coefficient) from OPN and AAOPN in a 2-D plane. Overlapping regions of OPN-based measures between N and PVC were greater compared to AAOPN-based measures. In OPN, N beat values exceeded those of PVC beats, while the reverse occurred in AAOPN. The performance of PVC recognition models (OPN-SVM, AAOPN-SVM, and HAOPN-SVM), trained on the MIT-BIH-AR database, is illustrated in Fig. 3(e). The metrics were obtained through fivefold cross-validation. The F_1 of OPN-SVM increased by approximately 4% to reach 90.17% in HAOPN-SVM. Se values of OPN-SVM and AAOPN-SVM were similar (86.85% and 86.62%), while HAOPN-SVM exhibited a boost to 91.77%. AAOPN-SVM achieved the highest PPV at 92.49%, while OPN-SVM’s was the lowest at 85.20%.

C. Influence of Parameters on PVC Classification

1) *Data Sampling Frequency:* The sampling frequency is a pivotal parameter that impacts both the dynamic information captured within the network and the size of the network, which influences computational efficiency. Thus, ECG signals were resampled across various frequencies, from 100 to 400 Hz (in increments of 50 Hz), to assess its impact on PVC recognition. Constructing CNs involved 0.1-s ECG segments centered on R peaks, with a time lag of $\tau = 1$, within the frequency range $F_s = [100:50:400]$ Hz.

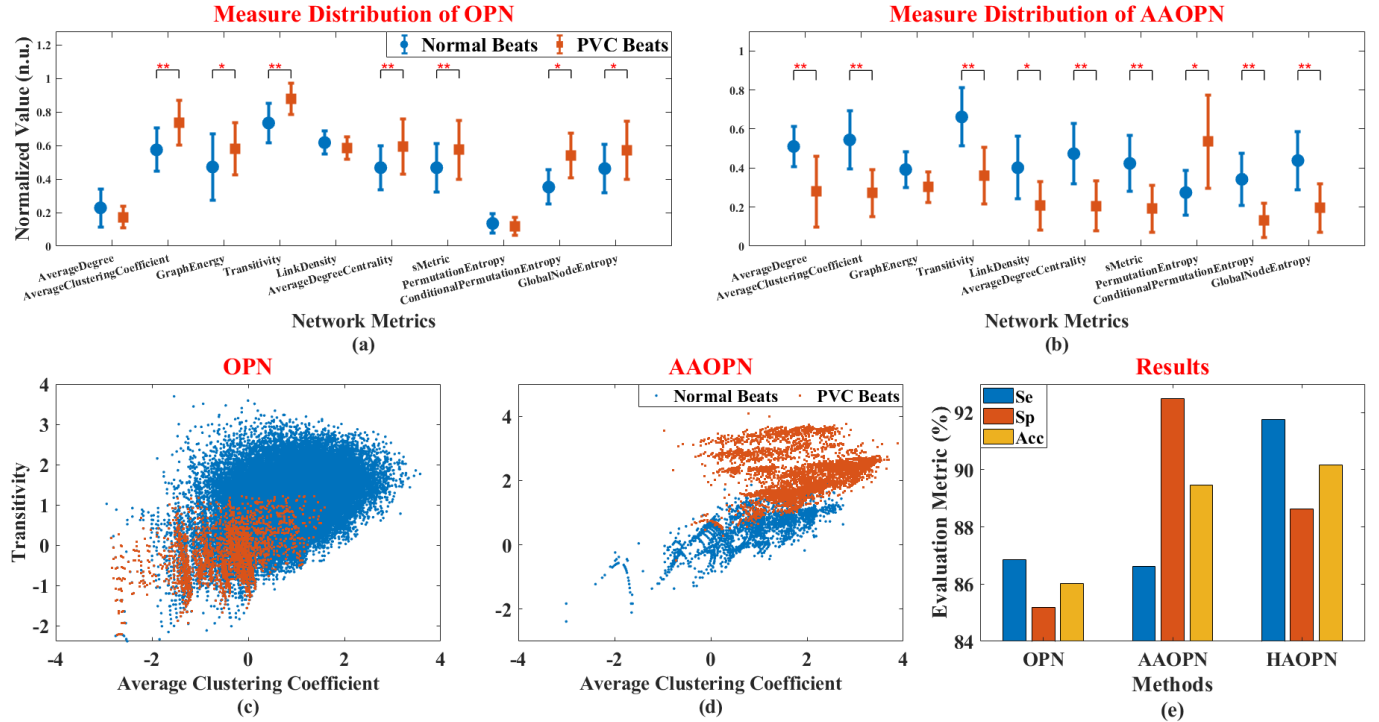


Fig. 3. PVC recognition performance of OPN, AAOPN, and HAOPN with $m = 5$, $\tau = 1$. (a) and (b) show the measure distribution of OPN and AAOPN, respectively, (c) and (d) are the distribution of two typical measures for OPN and AAOPN, respectively, and (e) demonstrate the PVC recognition performance of three models.

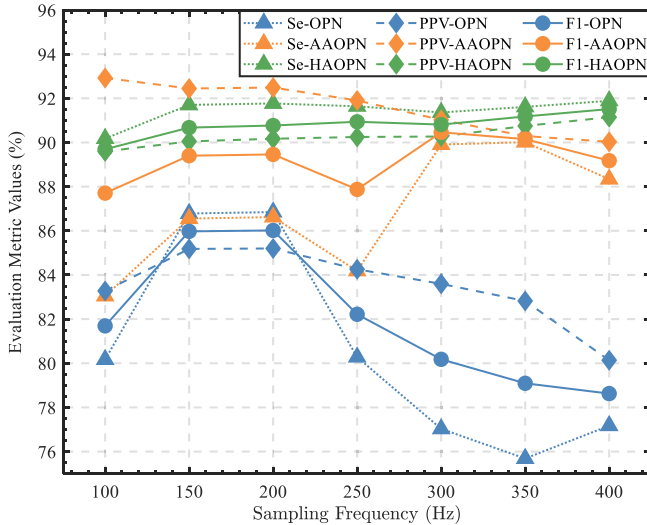


Fig. 4. PVC recognition results of three models under different sampling frequencies.

Fig. 4 portrays the PVC recognition outcomes of OPN-SVM, AAOPN-SVM, and HAOPN-SVM models using a class-oriented evaluation scheme. Generally, OPN-SVM exhibited an initial increase followed by a decrease in evaluation metrics, with an inflection point at 200 Hz. For AAOPN-SVM, as the frequency increased, PPV decreased, while Se and F_1 metrics fluctuated. Conversely, HAOPN-SVM metrics remained relatively stable across different frequencies.

This highlights that OPN-SVM and AAOPN-SVM are sensitive to signal temporal resolution, while HAOPN-SVM is less affected. Given the common ECG frequency range

of 0.05 to 100 Hz, an analog-to-digital converter sampling rate of 200 Hz aligns well with the Nyquist sampling theorem. Under this sampling rate, crucial frequency information can be retained during digitization. Consequently, subsequent experiments were performed on data resampled to 200 Hz.

2) *Data Length and Time Lag*: The choice of data length N and time lag τ significantly influenced the count of ordinal patterns ($N - (m - 1)\tau$) for a given m . The ensuing evaluation of PVC recognition performance for the three models across varying N and τ is depicted in Fig. 5, adopting a class-oriented scheme. The data length spanned $[0.1:0.1:0.5] * Fs$, while τ ranged from 1 to 9 with an increment of 2. Given the fixed Fs of 200 Hz from prior experiments, the horizontal axis in each Fig. 5 subfigure displayed the associated time length for each data length. Importantly, each evaluation metric for the three models shared a common color bar, with the color bar range being determined by the minimum and maximum values of results obtained across different conditions for the three models.

Overall, the HAOPN-SVM model exhibited superior performance across all three metrics. Concerning data length, OPN-SVM metrics declined as data length increased, whereas Se and F_1 of AAOPN-SVM peaked at $N = 0.2 * Fs$, and then dropped until $N = 0.4 * Fs$, showing the inverse pattern as PPV. HAOPN-SVM metrics spiked from $N = 0.1 * Fs$ to $N = 0.2 * Fs$ and remained stable thereafter. Regarding time lag, although all models displayed fluctuations, the overall impact was minimal. To attain optimal PVC recognition accuracy, the three models were ultimately trained on the MIT-BIH-AR database with parameters $N = 0.1 * Fs$, $\tau = 3$,

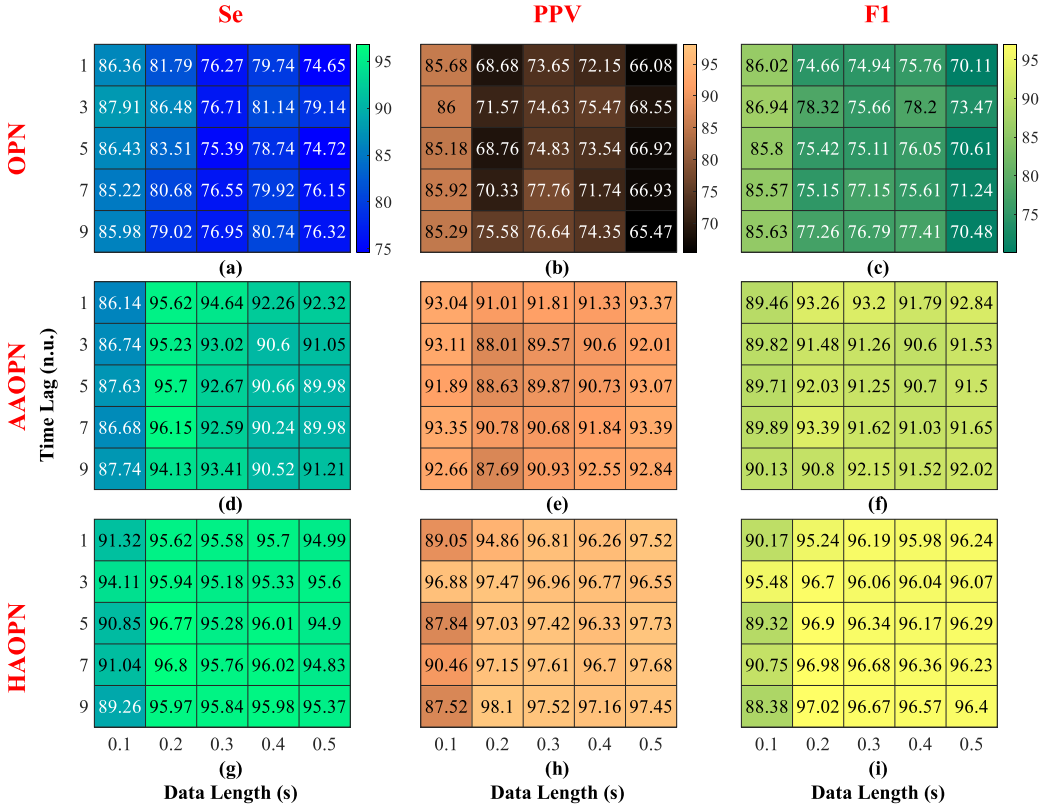


Fig. 5. Influence of data length and time lag on PVC recognition. The Se for OPN-SVM, AAOPN-SVM, and HAOPN-SVM are demonstrated in [(a), (d), and (g)] first column subfigures, and PPV, F_1 are depicted in [(b), (e), and (h)] second and [(c), (f), and (i)] third column subfigures.

$N = 0.2 * \text{Fs}$, $\tau = 7$, $N = 0.2 * \text{Fs}$, $\tau = 9$, respectively, and subsequently tested on the INCART and CPSC2020 databases.

D. Performance of OPN-Based Methods on PVC Recognition

1) *Compare With State-of-the-Art Works:* The OPN-based methods, originally designed for morphological abnormal ECG recognition, have been effectively applied to PVC identification. Their performance in a class-oriented scheme was evaluated and compared to state-of-the-art approaches on both the MIT-BIH-AR and INCART databases (see Table II). For the MIT-BIH-AR database, the proposed OPN-based PVC recognition methods demonstrated superiority over most existing approaches, with the HAOPN-SVM model achieving particularly high Se and PPV.

While the Se of our methods may not be exceptionally high, the PPV of the HAOPN-based method exceeded that of most existing methods. Additionally, AAOPN-SVM exhibited a more substantial enhancement in Se compared to OPN-SVM, and HAOPN-SVM improved PPV while maintaining a high Se. For the INCART database, the HAOPN-SVM model performed comparably or better than most state-of-the-art approaches, although OPN-SVM and AAOPN-SVM were not as competitive. Notably, these results were consistent across both databases, indicating the robustness of the proposed methods.

2) *Evaluations Between Class-Oriented and Subject-Oriented Experiments:* The performance of the proposed PVC classification methods was assessed using two evaluation

schemes: class-oriented and subject-oriented. In the class-oriented scheme, results for the MIT-BIH-AR and INCART databases are presented in Table II. For the subject-oriented scheme, results for the DS2 dataset and INCART database are shown in Table III. Compared with a class-oriented scheme, the Se of the HAOPN-SVM model from a subject-oriented scheme decreased by $\sim 5\%$ to 90.99% on MIT-BIH-AR/DS2 database and by $\sim 10\%$ to 82.35% on INCART database. Additionally, the F_1 exhibited a 3%–5% reduction on these databases, highlighting that the class-oriented scheme yielded more optimistic results than the subject-oriented scheme.

3) *Test on CPSC2020 Database:* Table IV presents the results of the proposed methods (with parameter settings listed in Table II) on the training set of CPSC2020. These methods exhibited reduced PVC recognition performance on wearable signals (CPSC2020-Train), whether in class-oriented or subject-oriented schemes. HAOPN-SVM exhibited the best performance, maintaining an overall F_1 above 90% in a class-oriented scheme. OPN-SVM was the most susceptible to wearable-associated noises, its F_1 decreased from 86.94% to 73.70% in a class-oriented scheme. Interestingly, in most cases, the reduction in three evaluation metrics was less pronounced in the subject-oriented scheme than in the class-oriented scheme.

To assess our methods on CPSC2020, we calculated the PVC scores based on the competition's scoring standards, where a false positive detection scores one point, and a false negative detection scores five points. The scores were computed for models trained on both the MIT-BIH-AR database

TABLE II
COMPARISON OF PVC RECOGNITION BETWEEN PROPOSED AND EXISTING METHODS ON MIT-BIH-AR DATABASE

Author	Class and focus	Method	Database	# Total beats	# PVC beats	Se (%)	PPV (%)	F_1 (%)
Llamedo, 2012 [34]	N, S, V, Q	Features-Automatic		90,089	7,809	82.00	70.00	—
		Features-Assisted				93±1	95±1	—
Teijeiro, 2016 [35]	N, S, V, F	Features+Rules	—	—	—	91.27	92.30	91.87
Yasin, 2018 [36]	PVC, Normal	Features+NN	—	81,844	7,122	95.13	—	—
Arrais, 2018 [37]	PVC, Normal	Redundant Discrete Wavelet Transform+Rules	—	80,872	3,408	99.18	99.15	—
Sokolova, 2019 [4]	PVC, Non_PVC	Features+Rules	MIT-BIH-AR	109,494	7,130	82.70	82.97	—
Malek, 2020 [5]	PVC, Normal	Template Matching+Rules	—	—	—	92.01	—	—
Yu, 2021 [38]	PVC, Normal	Deep Metric Learning+K-Nearest Neighbor	—	74,907	5,399	97.45	98.26	—
Mazidi, 2022 [39]	PVC, Normal	Features+KNN	—	49,219	2,851	98.23	—	—
		OPN+SVM ($F_s = 200 \text{ Hz}$, $\tau = 3$, $N = 0.1 * F_s$)	—	—	—	87.91	86.00	86.94
This study, 2022	PVC, Normal	AAOPN+SVM ($F_s = 200 \text{ Hz}$, $\tau = 7$, $N = 0.2 * F_s$)	96,587	6,983	96.15	90.78	93.39	—
		HAOPN+SVM ($F_s = 200 \text{ Hz}$, $\tau = 9$, $N = 0.2 * F_s$)	—	—	—	95.97	98.10	97.02
Llamedo, 2012[34]	N, S, V, Q	Automatic	—	153,651	20224	83.00	67.00	—
		Assisted by Expert	—	—	—	94±1	96±1	—
Li, 2015 [3]	PVC, Non_PVC	Template Matching	—	175,892	20,011	93.70	82.80	—
Oster, 2015 [40]	PVC, Non_PVC	Switching Kalman filters with no X-factor	—	175,871	20,011	95.40	99.30	97.30
Rahhal, 2018 [41]	PVC, Normal	Stacked Denoising Autoencoders+DNN	—	—	—	85.20	80.90	92.00
Sokolova, 2019 [4]	PVC, Non_PVC	Features+Rules	INCART	175,889	20,011	92.87	97.03	—
Malek, 2020 [5]	PVC, Normal	TM+Rules	—	—	—	91.14	—	—
Kalidas, 2020 [42]	PVC, Non_PVC	Semisupervised Autoencoder+Random Forests	—	175,674	19,990	88.08	94.76	91.30
Malik, 2021 [43]	PVC, Non_PVC	Features+AdaBoost	—	155,888	20,011	88.93	95.42	92.06
		OPN+SVM ($F_s = 200 \text{ Hz}$, $\tau = 3$, $N = 0.1 * F_s$)	—	—	—	68.83	88.34	77.38
This study, 2022	PVC, Normal	AAOPN+SVM ($F_s = 200 \text{ Hz}$, $\tau = 7$, $N = 0.2 * F_s$)	156,373	18,362	84.42	95.51	89.62	—
		HAOPN+SVM ($F_s = 200 \text{ Hz}$, $\tau = 9$, $N = 0.2 * F_s$)	—	—	—	92.55	93.58	93.06

TABLE III
PVC RECOGNITION RESULTS OF CLASS-ORIENTED AND SUBJECT-ORIENTED SCHEMES

Train Database	Test Database	Model	Se (%)	PPV (%)	F_1 (%)
DS1	DS2	OPN+SVM	69.67	88.11	77.81
		AAOPN+SVM	89.25	94.36	91.73
		HAOPN+SVM	90.99	98.44	94.57
	INCART	OPN+SVM	63.21	94.44	75.73
		AAOPN+SVM	77.44	93.42	84.68
		HAOPN+SVM	82.35	94.38	87.96

TABLE IV
PVC RECOGNITION PERFORMANCE ON CPSC2020-TRAIN DATABASE

Train Database	Model	Se (%)	PPV (%)	F_1 (%)
MIT-BIH-AR	OPN+SVM	76.03	71.51	73.70
	AAOPN+SVM	83.33	89.58	86.34
	HAOPN+SVM	90.65	91.41	91.03
DS1	OPN+SVM	63.78	80.51	71.18
	AAOPN+SVM	72.86	93.75	81.99
	HAOPN+SVM	83.44	95.09	88.89

and the CPSC2020-Train database, and compared with the top five teams on the hidden test set (see Table V). For models trained on the MIT-BIH-AR database, the best PVC score achieved by HAOPN-SVM was 53 904 on the hidden dataset and 17 052 on the training dataset, securing the second rank on CPSC2020-Test. To ensure a fair comparison with other competitors, models were also trained on the CPSC2020-Train database for PVC score calculation. As shown in Table V, while the scores decreased substantially on the CPSC2020-Train, there was a slight increase on the CPSC2020-Test. Notably, the results demonstrated that the proposed HAOPN-SVM method exhibited significant potential for PVC recognition in dynamic ECG monitoring.

TABLE V
PVC SCORES ON CPSC2020 DATABASE

Code No.	Method	CPSC2020-Train	CPSC2020-Test
CPSC1077	DenseNet+Rules	—	41,479
CPSC1091	DL-based+Rules	16,467	55,706
CPSC1093	Bi-LSTM	6,370	95,900
CPSC1082	WT+DL-based	4,482	97,913
CPSC1089	CNN	11,086	142,228
This work (Trained on MIT-BIH-AR database)	OPN+SVM	23,967	69,386
	AAOPN+SVM	19,336	57,238
	HAOPN+SVM	17,052	53,904
This work (Trained on CPSC2020-Train database)	OPN+SVM	9,684	82,522
	AAOPN+SVM	7,013	67,760
	HAOPN+SVM	5,371	59,201

IV. DISCUSSION

Accurate cardiac diagnosis necessitates innovative strategies for extracting nonlinear dynamics from ECG morphology and rhythm. CNs, particularly OPN, provide insights into nonlinear time series analysis through parameter-free symbolization. To overcome OPN's amplitude suppression limitation, we introduced AAOPN for amplitude-related information. We further integrated OPN and AAOPN measures into HAOPN, creating a comprehensive approach to enhance PVC recognition.

A. Performance Analysis of Proposed Algorithms

1) Comparison of OPN and AAOPN and Their Mapping to ECG Morphology: The variance in ordinal pattern definitions leads to disparate node number calculations, influenced by the embedding dimension m and coarse-grained symbol number $\alpha:m!$ for OPN and α^m for AAOPN. To ensure comparability between OPN and AAOPN network sizes, m and α were set to 5 and 2, respectively, resulting in $5! = 120$ and

$10^2 = 100$ nodes, creating a standardized basis for meaningful comparisons.

Both methods were applied and compared on typical N beats and PVC beats (see Fig. 2). Despite OPN having a larger number of possible nodes than AAOPN ($120 > 100$), the number of effective nodes was greater in AAOPN, particularly in PVC beats. This indicated that AAOPN captured a richer diversity of patterns and information. Compared to OPN, AAOPN exhibited higher degrees for nodes with the same symbol, signifying that more state retention information was encoded in the network. These encoded holding states represented characteristic sub-waves in the original ECG waveform, with transition states between them signifying the shifts between these sub-waves. Moreover, the transition states in OPN were fewer than those in AAOPN, suggesting that state transitions in OPN occurred more rapidly. This was related to the slope of the QRS complexes and corresponded to the width of the QRS complexes.

2) *Parameter Influence Analysis:* The temporal resolution affects the quantity of information from time series [44], therefore, we examined how sampling frequency affected OPN-based PVC identification models (see Fig. 4). In contrast to Myers's findings in distinguishing periodic from chaotic time series, OPN-SVM's PVC detection accuracy did not increase with greater sampling frequency [45]. Their OPN was calculated using long-term time series (many seconds of ECG signals) to ensure adequate effective nodes, whereas ours was calculated from a single ECG beat to differentiate morphological problems between beats. Since the positive and negative linear ordinal patterns ("0|1|2|3|4" and "4|3|2|1|0") had higher degrees than other ordinal patterns, our OPN's sequential patterns were sufficient. According to Fig. 4, AAOPN-SVM performed better than OPN-SVM and worse than HAOPN-SVM as sampling frequency increased. With higher sampling frequency, the segment utilized to build OPN and AAOPN ordinal patterns included shorter temporal information. The amplitude ordering was vulnerable to disturbances as temporal resolution grew, making OPN ordinal patterns inconstant. The holding states recorded by coarse-graining kept the AAOPN ordinal patterns constant. Therefore, HAOPN performed better since it had more segment shape and amplitude information.

To define the final parameters, data length and time lag on PVC identification were examined. The evaluation metrics (Se, PPV, and F_1) of OPN-SVM dropped with data length, while those of AAOPN-SVM first grew and subsequently fell with $N = 0.2 * F_s$ as the turning point. The reason may be that longer data tended to increase existing nodes rather than effective nodes. The evaluation metrics of HAOPN-SVM first increased and then stabilized, indicating that the time series with $N = 0.2 * F_s$ was sufficient to capture the necessary morphological information for PVC recognition. Owing to the symmetry of the QRS complex and T wave and the intrinsic characteristic of OPN and AAOPN, these models' assessment metrics seldom altered with time lag. QRS complexes and T waves are characterized by quasi-symmetric ascending and descending subwaves. As a result, the shape information mapped into OPN mainly represented positive and negative

linear ordinal patterns, which were independent of τ during the raising and lowering process. Similarly, AAOPN's resilience against τ was enhanced by the tiny embedding dimension, which was linked to the quasi-symmetric structure of QRS complexes and T wave.

B. Advantages Over Existing Algorithms

Compared with ES and DL-based methods, OPN and AAOPN-based measures could reflect temporal evolution and amplitude-related state transition of ECGs. To our knowledge, the proposed OPN-based PVC recognition framework in this article was the first to adopt CN for ECG heartbeat classification. Table II shows that the suggested HAOPN-SVM model performed similarly to state-of-the-art PVC identification.

In the MIT-BIH-AR database, a CNN-autoencoder-based feature extraction procedure and a random forest classifier achieved a high Se (99.07%) for PVC detection [46], but the high computational complexity and lack of physical or medical interpretation limited its clinical applications. A rule-based classifier could automatically classify multilead ECGs using morphological and rhythmic characteristics extracted from the abductive interpretation and a context-based adaptive QRS clustering technique [35]. The performance for four type beats (N, S, V, F) classification were $Se = 91.27\%$, $PPV = 92.30\%$, and $F_1 = 91.87\%$. Their satisfactory results were attributed by two factors: 1) multilead clean ECG signal monitoring, which was challenging under dynamic conditions and 2) precise feature points identification for accurate feature extraction (wave durations, intervals, amplitudes, etc.), which also poses difficulties in noisy environments. A deep metric learning model by Yu et al. [38] automatically extracted spatial information from heartbeats, and the KNN-based PVC identification classifier outperformed earlier investigations. Oppositely, our approach encodes both morphological and temporal information into CNs, attempting to enhance the interpretability of model features. Malek et al. [5] proposed an improved template-matching method for PVC recognition, their Se, Sp, and Acc on part (12 recordings) of MIT-BIH-AR database were 92.01%, 99.24%, and 98.84%, respectively. The accurate identification of noise-sensitive morphological traits (P -wave, Q -wave, T -wave, etc.) led to their great performance.

The proposed method was compared with existing approaches on the INCART database to assess its generalizability. A fully data-adaptive PVC recognition technique based on two beat-to-beat template-matching processes by Li et al. [3] performed $Se = 93.7\%$ and $PPV = 82.8\%$. However, template-matching methods are known for their sensitivity to large waveform distortions, a common occurrence in clinical practice, especially with ambulatory ECG signals. A switching Kalman filter was used to track several morphologies for manual annotation by a cardiologist, and unknown morphologies (X-Factor) were included to improve performance [40]. While achieving high performance, this method heavily relied on expert labeling and precise R-peak detection, limiting its suitability for real-time applications. Malik et al. [43] introduced a novel beat morphology feature

that represents the distance to the median beat in the recording and an unsupervised subject-specific normalization approach to detect ventricular ectopy by an AdaBoost classifier. Like most traditional handcrafted feature extraction methods, their performance was susceptible to variations in ECG signal quality, particularly in complex monitoring environments.

C. Generalization Capability to Wearable Signals

To evaluate the generalization and anti-noise capacity, the proposed method was tested on the CPSC2020-Train database (see Table IV). The results from the class-oriented scheme on CPSC2020-Train demonstrated that the HAOPN-SVM method exhibited superior generalization and robustness compared to the other two OPN-based methods. The reason was that the ordinal patterns defined by inequalities were relatively robust to noise. In addition, the coarse-graining process in AAOPN enhanced resistance to observational noise [47]. However, results from the subject-oriented scheme were less satisfactory, implying that class-oriented evaluation yielded more optimistic results. The underlying cause was that the training and testing databases had already been exposed to similar heartbeats from identical subjects. Furthermore, the performance of the proposed methods was also compared with the published top five teams of PVC recognition in the CPSC2020-Test database (see Table V). The published champion team employed the fusion of DenseNet and clinical rules-based refinement, almost all other teams adopted DL methods with parameter fine-tuning. Most of them could not generalize their excellent performance from the CPSC2020-Train to the CPSC2020-Test, indicating the overfitting problem of their models.

D. Limitations and Future Perspectives

Several limitations should be acknowledged in this investigation. The evaluation of the ECG morphological anomaly detection was limited to PVC beats. However, it is essential to validate the suggested methods on a wider range of ECG morphological abnormalities, including ventricular tachycardia, atrial flutter, and left/right bundle branch block, in order to ensure the reliability and generalizability of the findings. Furthermore, it should be noted that the time series utilized for the construction of OPNs solely relied on individual heartbeat data. This limited dataset may not provide sufficient duration for the accurate identification of block-type ECG morphological anomalies, such as type 2 second-degree atrioventricular block. It is advisable to investigate the inclusion of longer data sets, comprising multiple extended periods of heartbeats. Additionally, only the influence of sampling frequency is investigated, heart rate variations can introduce signal distortions or overlapping beats, potentially affecting the accuracy of arrhythmia detection. Frequency domain analysis is a potential solution to further enhance the robustness of our method in real-world clinical applications. While our approach does encode morphological and temporal information into CN and these network features can be correlated with clinical diagnostic information, we recognize that the level of interpretability in a clinical context may require further validation and collaboration with clinicians.

The proposed method holds promise for diverse applications in healthcare technology. Its real-time detection capabilities, especially in identifying PVC, make it valuable for healthcare monitoring systems, offering timely intervention for patients with heart conditions. Integration into wearable devices enhances their ability to monitor and detect cardiac anomalies, catering to individuals requiring continuous heart monitoring outside clinical settings. In telemedicine platforms, the method facilitates remote ECG signal monitoring, providing crucial feedback to healthcare professionals. Moreover, its versatility makes it suitable for medical diagnostics and research, contributing to comprehensive analyses of cardiac abnormalities. Collaboration with ECG device manufacturers offers the potential to integrate the method, providing users with more precise insights into their cardiac health.

V. CONCLUSION

In this study, we have proposed a novel PVC recognition method that leverages hybrid amplitude information, integrating shape-based data from OPNs and amplitude level-based data from AAOPNs. The SVM serves as an effective classifier in this framework. The methodology involves coarse-graining the original time series into symbolic series, followed by the conversion of both the original time series and symbolic series into embedded vectors and ordinal patterns based on the amplitude and chronological ordering of these vectors, respectively. Subsequently, OPNs and AAOPNs are constructed with the temporal succession of ordinal patterns as links. Our approach, utilizing a combination of network measures derived from both networks, demonstrates robustness and efficacy in training and testing SVM-based PVC recognition models.

The performance evaluation of our proposed model has been conducted using diverse clinical databases, including the Massachusetts Institute of Technology-Beth Israel Hospital arrhythmia database and the St. Petersburg Institute of Cardiological Technics database, as well as wearable databases, represented by the train and test sets of the China Physiological Signal Challenge 2020 database. The results showcase the superior potential of the HAOPNs-based SVM model compared to existing algorithms. Its application extends beyond clinical settings, as it proves to be a valuable tool for cardiac diagnosis assistance in daily-life telemonitoring applications. The versatility and robustness of our method position it as a significant advancement in cardiac signal processing, promising enhanced accuracy in PVC recognition and contributing to the advancement of telehealth and wearable technologies for cardiovascular monitoring.

REFERENCES

- [1] S. Chandra and R. Gupta, "Smart biomedical sensor network for multipatient cardiac arrhythmia monitoring," *IEEE Trans. Instrum. Meas.*, vol. 72, pp. 1–9, 2023, doi: [10.1109/TIM.2022.3231278](https://doi.org/10.1109/TIM.2022.3231278).
- [2] Y. Wu et al., "Clinical validation of a capacitive electrocardiogram cushion utilized for arrhythmias monitoring," *IEEE Trans. Instrum. Meas.*, vol. 72, pp. 1–13, 2023, doi: [10.1109/TIM.2023.3251392](https://doi.org/10.1109/TIM.2023.3251392).
- [3] P. Li, C. Liu, X. Wang, D. Zheng, Y. Li, and C. Liu, "A low-complexity data-adaptive approach for premature ventricular contraction recognition," *Signal, Image Video Process.*, vol. 8, no. 1, pp. 111–120, Jan. 2014, doi: [10.1007/s11760-013-0478-6](https://doi.org/10.1007/s11760-013-0478-6).

- [4] A. A. Sokolova et al., "Multi-parametric algorithm for premature ventricular contractions detection and counting," in *Proc. AIP Conf.*, vol. 2140, St. Petersburg, Russia, 2019, Art. no. 020074, doi: [10.1063/1.5121999](https://doi.org/10.1063/1.5121999).
- [5] A. S. Malek, A. Elnahrawy, H. Anwar, and M. Naeem, "Automated detection of premature ventricular contraction in ECG signals using enhanced template matching algorithm," *Biomed. Phys. Eng. Exp.*, vol. 6, no. 1, Jan. 2020, Art. no. 015024, doi: [10.1088/2057-1976/ab6995](https://doi.org/10.1088/2057-1976/ab6995).
- [6] Ö. Yıldırım, P. Plawiak, R.-S. Tan, and U. R. Acharya, "Arrhythmia detection using deep convolutional neural network with long duration ECG signals," *Comput. Biol. Med.*, vol. 102, pp. 411–420, Nov. 2018, doi: [10.1016/j.combiomed.2018.09.009](https://doi.org/10.1016/j.combiomed.2018.09.009).
- [7] P. Plawiak, "Novel methodology of cardiac health recognition based on ECG signals and evolutionary-neural system," *Expert Syst. Appl.*, vol. 92, pp. 334–349, Feb. 2018, doi: [10.1016/j.eswa.2017.09.022](https://doi.org/10.1016/j.eswa.2017.09.022).
- [8] J. Wang, "Automated detection of premature ventricular contraction based on the improved gated recurrent unit network," *Comput. Methods Programs Biomed.*, vol. 208, Sep. 2021, Art. no. 106284, doi: [10.1016/j.cmpb.2021.106284](https://doi.org/10.1016/j.cmpb.2021.106284).
- [9] C. Li, L. Mo, and R. Yan, "Fault diagnosis of rolling bearing based on WHVG and GCN," *IEEE Trans. Instrum. Meas.*, vol. 70, pp. 1–11, 2021, doi: [10.1109/TIM.2021.3087834](https://doi.org/10.1109/TIM.2021.3087834).
- [10] G. Zhu et al., "Brain injury localization and size estimation using electromagnetic symmetric crossing lines method," *IEEE Trans. Instrum. Meas.*, vol. 72, pp. 1–11, 2023, doi: [10.1109/TIM.2023.3295014](https://doi.org/10.1109/TIM.2023.3295014).
- [11] V. Godavarthi, S. A. Pawar, V. R. Unni, R. I. Sujith, N. Marwan, and J. Kurths, "Coupled interaction between unsteady flame dynamics and acoustic field in a turbulent combustor," *Chaos, Interdiscipl. J. Nonlinear Sci.*, vol. 28, no. 11, Nov. 2018, Art. no. 113111, doi: [10.1063/1.5052210](https://doi.org/10.1063/1.5052210).
- [12] N. Frolov et al., "Revealing a multiplex brain network through the analysis of recurrences," *Chaos, Interdiscipl. J. Nonlinear Sci.*, vol. 30, no. 12, 2020, Art. no. 121108, doi: [10.1063/5.0028053](https://doi.org/10.1063/5.0028053).
- [13] N. Makaram, P. A. Karthick, and R. Swaminathan, "Analysis of dynamics of EMG signal variations in fatiguing contractions of muscles using transition network approach," *IEEE Trans. Instrum. Meas.*, vol. 70, pp. 1–8, 2021, doi: [10.1109/TIM.2021.3063777](https://doi.org/10.1109/TIM.2021.3063777).
- [14] C. Masoller et al., "Quantifying sudden changes in dynamical systems using symbolic networks," *New J. Phys.*, vol. 17, no. 2, Feb. 2015, Art. no. 023068, doi: [10.1088/1367-2630/17/2/023068](https://doi.org/10.1088/1367-2630/17/2/023068).
- [15] Y. Zou, R. V. Donner, N. Marwan, J. F. Donges, and J. Kurths, "Complex network approaches to nonlinear time series analysis," *Phys. Rep.*, vol. 787, pp. 1–97, Jan. 2019, doi: [10.1016/j.physrep.2018.10.005](https://doi.org/10.1016/j.physrep.2018.10.005).
- [16] R. V. Donner et al., "Recurrence-based time series analysis by means of complex network methods," *Int. J. Bifurcation Chaos*, vol. 21, no. 4, pp. 1019–1046, Apr. 2011, doi: [10.1142/s0218127411029021](https://doi.org/10.1142/s0218127411029021).
- [17] C. Bandt and B. Pompe, "Permutation entropy: A natural complexity measure for time series," *Phys. Rev. Lett.*, vol. 88, no. 17, Apr. 2002, Art. no. 174102, doi: [10.1103/physrevlett.88.174102](https://doi.org/10.1103/physrevlett.88.174102).
- [18] L. D. Santos, D. C. Corrêa, D. M. Walker, M. F. de Godoy, E. E. N. Macau, and M. Small, "Characterisation of neonatal cardiac dynamics using ordinal partition network," *Med. Biol. Eng. Comput.*, vol. 60, no. 3, pp. 829–842, Mar. 2022, doi: [10.1007/s11517-021-02481-0](https://doi.org/10.1007/s11517-021-02481-0).
- [19] A. A. B. Pessa, R. S. Zola, M. Perc, and H. V. Ribeiro, "Determining liquid crystal properties with ordinal networks and machine learning," *Chaos, Solitons Fractals*, vol. 154, Jan. 2022, Art. no. 111607, doi: [10.1016/j.chaos.2021.111607](https://doi.org/10.1016/j.chaos.2021.111607).
- [20] J. Zhang, J. Zhou, M. Tang, H. Guo, M. Small, and Y. Zou, "Constructing ordinal partition transition networks from multivariate time series," *Sci. Rep.*, vol. 7, no. 1, pp. 1–13, Aug. 2017, doi: [10.1038/s41598-017-08245-x](https://doi.org/10.1038/s41598-017-08245-x).
- [21] X. Sun, M. Small, Y. Zhao, and X. Xue, "Characterizing system dynamics with a weighted and directed network constructed from time series data," *Chaos, Interdiscipl. J. Nonlinear Sci.*, vol. 24, no. 2, Jun. 2014, Art. no. 024402, doi: [10.1063/1.4868261](https://doi.org/10.1063/1.4868261).
- [22] ICBE Conference Organizing Committee. *Searching for Premature Ventricular Contraction and Supraventricular Premature Beat From Long-Term ECGs: The 3rd China Physiological Signal Challenge 2020*. Accessed: Jan. 16, 2024. [Online]. Available: <http://2020.icbeb.org/CSPC2020>
- [23] Z. Cai. (2024). *Annotations_CPS2020*. Accessed: Jan. 16, 2024. [Online]. Available: https://drive.google.com/drive/folders/1hobaSvZPW3nR_O0Q3soxLdLMiDhmbNzb?usp=drive_link
- [24] D. Lee et al., "Optimal lead position in patch-type monitoring sensors for reconstructing 12-lead ECG signals with universal transformation coefficient," *Sensors-Basel*, vol. 20, no. 4, p. 963, 2020, doi: [10.3390/s20040963](https://doi.org/10.3390/s20040963).
- [25] X. Wang, Y. Li, H. Gao, X. Cheng, J. Li, and C. Liu, "A causal intervention scheme for semantic segmentation of quasi-periodic cardiovascular signals," *IEEE J. Biomed. Health Informat.*, vol. 27, no. 7, pp. 3175–3186, Apr. 2023, doi: [10.1109/JBHI.2023.3270978](https://doi.org/10.1109/JBHI.2023.3270978).
- [26] C. León, G. Carrault, P. Pladys, and A. Beuchée, "Early detection of late onset sepsis in premature infants using visibility graph analysis of heart rate variability," *IEEE J. Biomed. Health Informat.*, vol. 25, no. 4, pp. 1006–1017, Apr. 2021, doi: [10.1109/JBHI.2020.3021662](https://doi.org/10.1109/JBHI.2020.3021662).
- [27] R. Balakrishnan, "The energy of a graph," *Linear Algebra Appl.*, vol. 387, pp. 287–295, Aug. 2004, doi: [10.1016/j.laa.2004.02.038](https://doi.org/10.1016/j.laa.2004.02.038).
- [28] Z. Liu, W. Dong, and Y. Fu, "Local degree blocking model for link prediction in complex networks," *Chaos, Interdiscipl. J. Nonlinear Sci.*, vol. 25, no. 1, Jan. 2015, Art. no. 013115, doi: [10.1063/1.4906371](https://doi.org/10.1063/1.4906371).
- [29] J. Zhang and Y. Luo, "Degree centrality, betweenness centrality, and closeness centrality in social network," in *Proc. 2nd Int. Conf. Modelling, Simulation Appl. Math. (MSAM2017)*, 2017, pp. 300–303, doi: [10.2991/msam-17.2017.68](https://doi.org/10.2991/msam-17.2017.68).
- [30] L. Li, D. Alderson, J. C. Doyle, and W. Willinger, "Towards a theory of scale-free graphs: Definition, properties, and implications," *Internet Math.*, vol. 2, no. 4, pp. 431–523, Jan. 2005, doi: [10.1080/15427951.2005.10129111](https://doi.org/10.1080/15427951.2005.10129111).
- [31] M. McCullough, M. Small, H. H. C. Iu, and T. Stemler, "Multiscale ordinal network analysis of human cardiac dynamics," *Phil. Trans. Roy. Soc. A, Math., Phys. Eng. Sci.*, vol. 375, no. 2096, Jun. 2017, Art. no. 20160292, doi: [10.1098/rsta.2016.0292](https://doi.org/10.1098/rsta.2016.0292).
- [32] J. West et al., "Differential network entropy reveals cancer system hallmarks," *Sci. Rep.*, vol. 2, no. 1, pp. 1–8, 2012, doi: [10.1038/srep00802](https://doi.org/10.1038/srep00802).
- [33] M. McCullough, M. Small, T. Stemler, and H. H.-C. Iu, "Time lagged ordinal partition networks for capturing dynamics of continuous dynamical systems," *Chaos, Interdiscipl. J. Nonlinear Sci.*, vol. 25, no. 5, May 2015, Art. no. 053101, doi: [10.1063/1.4919075](https://doi.org/10.1063/1.4919075).
- [34] M. Llamedo and J. P. Martinez, "An automatic patient-adapted ECG heartbeat classifier allowing expert assistance," *IEEE Trans. Biomed. Eng.*, vol. 59, no. 8, pp. 2312–2320, Aug. 2012, doi: [10.1109/TBME.2012.2202662](https://doi.org/10.1109/TBME.2012.2202662).
- [35] T. Teijeiro, P. Félix, J. Presedo, and D. Castro, "Heartbeat classification using abstract features from the abductive interpretation of the ECG," *IEEE J. Biomed. Health Informat.*, vol. 22, no. 2, pp. 409–420, Mar. 2018, doi: [10.1109/JBHI.2016.2631247](https://doi.org/10.1109/JBHI.2016.2631247).
- [36] Y. Kaya, "Classification of PVC beat in ECG using basic temporal features," *Balkan J. Electr. Comput. Eng.*, vol. 6, no. 2, pp. 78–82, Apr. 2018, doi: [10.17694/bajece.419541](https://doi.org/10.17694/bajece.419541).
- [37] E. Arrais Junior, R. A. D. M. Valentim, and G. B. Brandão, "Real-time premature ventricular contractions detection based on redundant discrete wavelet transform," *Res. Biomed. Eng.*, vol. 34, no. 3, pp. 187–197, Jul. 2018, doi: [10.1590/2446-4740.01618](https://doi.org/10.1590/2446-4740.01618).
- [38] J. Yu, X. Wang, X. Chen, and J. Guo, "Automatic premature ventricular contraction detection using deep metric learning and KNN," *Biosensors*, vol. 11, no. 3, p. 69, Mar. 2021, doi: [10.3390/bios11030069](https://doi.org/10.3390/bios11030069).
- [39] M. H. Mazidi, "Premature ventricular contraction (PVC) detection system based on tunable Q-factor wavelet transform," *J. Biomed. Phys. Eng.*, vol. 12, no. 1, pp. 61–74, Feb. 2022, doi: [10.31661/jbpe.v0i1.1235](https://doi.org/10.31661/jbpe.v0i1.1235).
- [40] J. Oster, J. Behar, O. Sayadi, S. Nemati, A. E. W. Johnson, and G. D. Clifford, "Semisupervised ECG ventricular beat classification with novelty detection based on switching Kalman filters," *IEEE Trans. Biomed. Eng.*, vol. 62, no. 9, pp. 2125–2134, Sep. 2015, doi: [10.1109/TBME.2015.2402236](https://doi.org/10.1109/TBME.2015.2402236).
- [41] M. M. A. Rahhal, N. A. Ajlan, Y. Bazi, H. A. Hichri, and T. Rabczuk, "Automatic premature ventricular contractions detection for multi-lead electrocardiogram signal," in *Proc. IEEE Int. Conf. Electro/Inf. Technol. (EIT)*, May 2018, pp. 169–173, doi: [10.1109/EIT.2018.8500197](https://doi.org/10.1109/EIT.2018.8500197).
- [42] V. Kalidas and L. S. Tamil, "Detection of premature ventricular complexes using semisupervised autoencoders and random forests," in *Proc. 42nd Annu. Int. Conf. IEEE Eng. Med. Biol. Soc. (EMBC)*, Jul. 2020, pp. 337–340, doi: [10.1109/EMBC44109.2020.9176054](https://doi.org/10.1109/EMBC44109.2020.9176054).
- [43] J. Malik, Z. Loring, J. P. Piccini, and H.-T. Wu, "Interpretable morphological features for efficient single-lead automatic ventricular ectopy detection," *J. Electrocardiol.*, vol. 65, pp. 55–63, Mar. 2021, doi: [10.1016/j.jelectrocard.2020.11.014](https://doi.org/10.1016/j.jelectrocard.2020.11.014).
- [44] G. Iacobello et al., "A review on turbulent and vortical flow analyses via complex networks," *Phys. A, Stat. Mech. Appl.*, vol. 563, Feb. 2021, Art. no. 125476, doi: [10.1016/j.physa.2020.125476](https://doi.org/10.1016/j.physa.2020.125476).

- [45] A. Myers, E. Munch, and F. A. Khasawneh, "Persistent homology of complex networks for dynamic state detection," *Phys. Rev. E, Stat. Phys. Plasmas Fluids Relat. Interdiscip. Top.*, vol. 100, no. 2, Aug. 2019, Art. no. 022314, doi: [10.1103/physreve.100.022314](https://doi.org/10.1103/physreve.100.022314).
- [46] M. Gordon and C. Williams, "PVC detection using a convolutional autoencoder and random forest classifier," in *Proc. Biocomputing*, Nov. 2018, pp. 42–53, doi: [10.1142/9789813279827_0005](https://doi.org/10.1142/9789813279827_0005).
- [47] J. M. Amigó, K. Keller, and V. A. Unakafova, "Ordinal symbolic analysis and its application to biomedical recordings," *Phil. Trans. Roy. Soc. A, Math., Phys. Eng. Sci.*, vol. 373, no. 2034, Feb. 2015, Art. no. 20140091, doi: [10.1098/rsta.2014.0091](https://doi.org/10.1098/rsta.2014.0091).



Zhipeng Cai (Member, IEEE) received the B.S. degree in measurement and control technology and instruments from the School of Mechanical Engineering, Jiangsu University, Zhenjiang, China, in 2013, and the M.S. and Ph.D. degrees from the School of Instrument Science and Engineering, Southeast University, Nanjing, China, in 2015 and 2019 respectively, where he is currently pursuing the Ph.D. degree in instrument science and technology.

His research interests include bio-signal processing, intelligent monitoring systems, and network physiology.



Caiyun Ma (Graduate Student Member, IEEE) received the M.S. degree in biomedical engineering from Shandong University, Jinan, China, in 2020. She is currently pursuing the Ph.D. degree in instrument science and technology with Southeast University, Nanjing, China.

Her research interests include physiological signals processing and atrial fibrillation signals classification using machine learning.



Jianqing Li (Senior Member, IEEE) received the B.S. and M.S. degrees in automatic technology from the School of Instrument Science and Engineering, Southeast University, Nanjing, China, in 1986 and 1992 respectively, and the Ph.D. degree in measurement technology and instruments from Southeast University, in 2000.

He is currently a Professor and a Vice President at the School of Basic Medical Sciences, Nanjing Medical University, Nanjing. He is also a Professor at the School of Instrument Science and Engineering,

Southeast University. His research interests include mHealth and wireless networks.



Chengyu Liu (Senior Member, IEEE) received the B.S. and Ph.D. degrees in biomedical engineering from Shandong University, Jinan, China, in 2005 and 2010, respectively.

He has completed post-doctoral training at Shandong University from 2010 to 2013; Newcastle University, Newcastle upon Tyne, U.K., from 2013 to 2014; and Emory University, Atlanta, GA, USA, from 2015 to 2017. He is currently a Professor with the School of Instrument Science and Engineering, Southeast University, Nanjing, China, where he is also the Director of the Southeast-Lenovo Wearable Heart-Sleep-Emotion Intelligent Monitoring Laboratory. He has published more than 100 papers, eight chapters in books, and 15 invention patents. His research interests include mHealth and intelligent monitoring, machine learning and big data processing for cardiovascular signals, device development for CADs, and sleep and emotion monitoring.

Dr. Liu is now a Federation Journal Committee Member of the International Federation for Medical and Biological Engineering (IFMBE). He was the PI for more than ten awarded grants.